Tensorial x-ray structure factor in smectic liquid crystals

Anne-Marie Levelut and Brigitte Pansu
Laboratoire de Physique des Solides, CNRS/UPS UMR No. 8502, Université Paris–Sud, F-91405 Orsay Cédex, France
(Received 22 February 1999)

The amplitudes and the polarizations of the different resonant reflections characterizing the modulation of the orientational order in smectic liquid crystals are derived from the molecular tensorial structure factor. In the case of a commensurate helicoidal modulation, our conclusions are consistent with the previous predictions of Dimitrienko. We have extended Dimitrienko's prediction to incommensurate helicoidal structures and to commensurate but nonhelicoidal modulations. We have compared the estimated values for different models of modulations with the same period, with the experimental data obtained on different smectic-*C* variants. These comparisons enable us to discriminate between the different models. [S1063-651X(99)12511-X]

PACS number(s): 61.30.Eb

I. INTRODUCTION

A. The role of the chirality in the polymorphism of mesogenic molecules

By introducing some chirality into the components of a mesophase, one favors the occurrence of twisting forces which can modify the usual uniform orientational order. For example, the positional order of the molecules in a nematic phase is that of a usual liquid, but the molecular orientations are distributed around a preferred axis, the so-called director **n**. In this case, the substitution of chiral molecules for achiral ones does not locally modify the nematic organization, but creates instead an overall helical ordering of the local director. The helical axis is perpendicular to **n** and the pitch is generally in the range of 0.3–10 μm. Similarly, in smectic phases, where rodlike molecules are organized into fluid stacks of planar layers, weak chiral twisting forces induce a helical order with the helical axis parallel to the layer normal. Such helical order is only achieved when the director possesses a component in the layer plane, i.e., in the smectic-*C* (Sm*C*) phase, where **n** is tilted with respect to the layer normal. In the helically ordered smectic-*C* phase, the tilt angle is the same in all the layers but the direction of the in-plane projection of the director, **c**, differs by a constant angle $\Delta\psi$ from one layer to the next; this structure is called the chiral smectic-*C* (Sm*C**) phase. In general, $\Delta\psi$ is in the range of $\pm 5°$ (here the different signs indicate the two possible senses of helix handedness). The resulting helical pitch is in the optical wavelength range. Moreover, the symmetry properties of each layer are consistent with the existence of a spontaneous polarization parallel to the smectic plane and perpendicular to **n** [1]. If the pitch is large, it is easy to unwind the helix by the application of a weak strain, imposed, for example, by suitable anchoring conditions on a rigid surface or by a weak applied electric field. Then the sample has a ferroelectric response under moderate applied electric fields.

If the twisting power is increased, the nature of the mesophases becomes different. For example, in the nematic phase there is a tendency for developing helical order in any direction perpendicular to the director. This tendency generates a geometrical frustration which is resolved by a three dimensional network of disclination lines organized on a cubic lattice, with a lattice constant in the optical wavelength range [2]. The crystalline character of these phases is responsible for the brightly colored appearance of the single crystals, from which the designation of ''blue phases'' is derived.

In smectic phases, the competition between a helical ordering developing parallel to the smectic planes and the layer ordering can induce the formation of a periodic array of twist grain boundaries (TGB phases) [3]. Starting from a smectic-*A* phase, where the director is parallel to the layer normal, one can obtain a TGBA phase, in which a set of parallel and equidistant grain boundaries divide the smectic structure into equal thickness slabs with smectic A organization. The layer normal of each slab is parallel to the grain boundaries, but its orientation changes by a constant angle across each grain boundary. Similar TGBC phases exist, but the grain boundaries in these phases are not necessarily perpendicular to the layer planes; moreover an additional helical ordering around an axis parallel to the layer normal is also allowed by the local symmetry properties of each smectic slab.

In addition to the above cases, different Sm*C** variants with a simple, lamellar Sm*C*-type of structure (Fig. 1) have been detected by differential scanning microscopy and electro-optical studies [4]. In these Sm*C** variants, a transition to a ferroelectric Sm*C* structure is observed under high electric fields, but at lower fields the response is either antiferroelectric or ferrielectric. This diversity in the electro-optical behavior is certainly related to short-period modulations of the direction of spontaneous polarization and of the

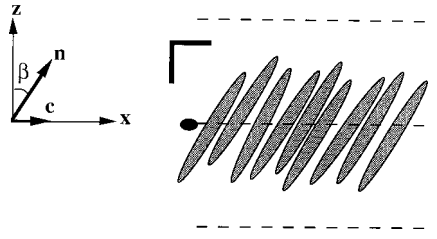

FIG. 1. Schematic representation of a smectic-*C* layer with its symmetry elements (represented by their usual symbols [8]). The mirror plane is suppressed if the layer is made of chiral molecules. In this case, the electric dipole is parallel to the binary axis (*y*).

orientational order. Finally, a few chiral mesogenic molecules exhibit structures that are crystals of defects (the SmQ phase), confirming that the orientational order can indeed be modulated over short periods (two to four molecular lengths) [5].

B. Methods of structural investigation of chiral mesophases

The structural investigation of chiral phases with a large pitch can be performed by diffraction experiments in the visible light wavelength range (for the blue phases) [6], or by a combination of direct optical observations with x-ray-diffraction studies (for the TGB phases). In the SmQ phases, the combination of the short-period and the three-dimensional character induces a coupling between orientational and positional order. Indeed, this is the only case where the structure of a short-period chiral mesophase has been solved by conventional x-ray-diffraction methods. Apart from one of them (SmC_A^*), which has antiferroelectric properties, the *a priori* simpler layer structures of the chiral smectic-C variants were not well established until the recent resonant x-ray-diffraction experiments [7].

In fact, whereas visible light couples to the orientation of molecules via the local dielectric tensor, conventional x-ray-diffraction methods are only sensitive to density modulations (in other words, the susceptibility is a scalar quantity). Because of this lack of sensitivity to modulation of orientational order, a short pitch organization (for example in antiferroelectric phases) is usually invisible by x-ray-diffraction methods. Let us illustrate this point by considering the case of crystalline networks with helical symmetry [8]. In some crystals, the contents of the unit cell can be divided into smaller identical subunits. These subunits, called asymmetric units, are related to one another by an operation product of a rotation R and of a translation T. In order to preserve the periodic nature of the crystalline order, the operation $(RT)^N$ must correspond to an elementary lattice translation. Therefore, R is a rotation of $2\pi/N$ with $N=2,3,4,6$, or a mirror symmetry $(\overline{2})$. If the rotation axis is parallel to z, and if C is the corresponding lattice parameter, the translation T is $n\vec{C}/N$, where n is an integer; here $n<N$. The corresponding symmetry element is called a *nonsymmorphic element*, glide plane, or helical axis. The helical axes are labeled N_n. As a consequence of the relation $\vec{C}(n/N)\equiv-\vec{C}(N-n)/N$ modulo $\vec{C}$, N_n and N_{N-n} are equivalent but of opposite handedness.

In the following discussion we will take the example of an N_1 axis. Perpendicular to the z axis, the crystal is divided into N sublayers, which are all equivalent modulo a rotation of $2\pi/N$ around z. With a scalar structure factor, the different sublayers are indistinguishable by an x-ray-diffraction experiment. Therefore, the period along z appears to be C/N instead of C. The corresponding apparent periodicity along the reciprocal z axis is NC^*, while the apparent periodicity along any other reciprocal rod parallel to z is not disturbed by the presence of a nonsymmorphic element. This could be expressed by the following extinction rules: $F(0,0,l)=0$ if $l\neq Nl'$, where l' and l are integers; there are no restrictions on $F(h,k,l)$ if h or $k\neq 0$ (Fig. 2).

The extinction rules can easily be extended to crystals with incommensurate helical order, as, for example, in crystalline phases of polypeptides [9]. In an incommensurate helical structure, two colinear periods coexist along the z axis. The smaller one, C, corresponds to the period of distribution of the asymmetric subunits, while the larger period P corresponds to the pitch. There are two kind of nodes in the reciprocal network: The fundamental nodes $(h,k,l,0)$ with a z^* coordinate $lC^*=2\pi l/C$, and the satellites (h,k,l,m) $(m\neq 0)$ with a z^* coordinate equal to $lC^*+2\pi m/P$ with h,k,l,m integers. The helical structure implies no restriction on $F(h,k,l,m)$ with h or $k\neq 0$, but $F(0,0,l,m)=0$ if $m\neq 0$. Hence, along the z reciprocal axis $(h=k=0)$ the period is $2\pi/C$, whereas the pitch periodicity appears only along reciprocal space directions which are parallel to the z axis but not coincident with it.

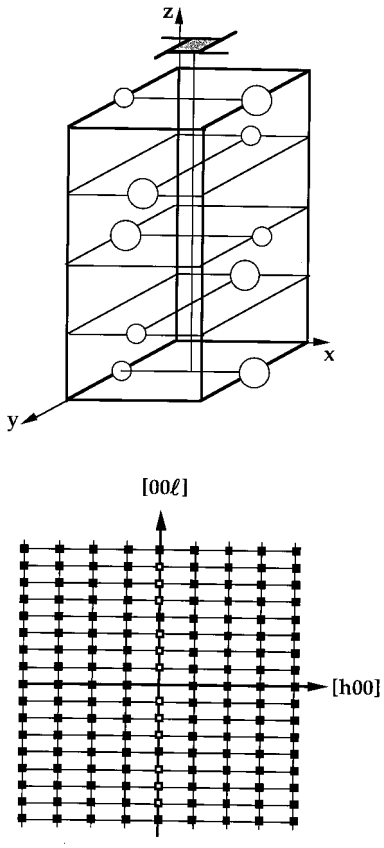

FIG. 2. Top: example of a tetragonal unit cell with a 4_1 symmetry axis. Bottom: the reciprocal $h0l$ plane; open squares mark the position of the usually forbidden reflections and full squares mark the nodes which are observed at any energy.

In smectic liquid crystals, there is no correlation between the in-layer (i.e., x-y plane) positions of molecules belonging to different layers, therefore there are no (h,k,l) reflections with $l\neq 0$ at the same time that h or $k\neq 0$. Depending on the intralayer structure, some sharp peaks can be seen in the $(h,k,0)$ reciprocal plane. In any case, the absence of (h,k,l) reflections makes it impossible to obtain direct evidence (by conventional x-ray diffraction) of the helical symmetry. Moreover, in the absence of three-dimensional (3D) periodicity there is no restriction on the rotation symmetry R (N can take any value).

By operating at an x-ray energy close to an absorption edge of one of the atoms in the considered material, we are probing a resonance condition. The coupling between the

electromagnetic radiation and the electronic cloud results in a tensorial atomic scattering factor. In other words, the polarization direction and the phase of the scattered wave depends on the nature and orientation of the bond environment close to the resonantly scattering atom. Therefore, a modulation of orientational order results in diffraction peaks which are otherwise forbidden in a conventional x-ray-diffraction experiment. Such forbidden diffraction peaks have been observed at the Br *K* edge in a single crystal of sodium bromate [10]. Moreover, a study of the absorption spectra of several other compounds, as well as a crystal structure determination, have been performed using the resonant scattering technique [11].

C. Resonant diffraction experiments in smectic-*C* variants: A tool for discrimination between different models

In the absence of associated 3D translational order (as is present in the Sm*Q* phase), resonant x-ray scattering is a general method that can reveal the short-period orientational modulations of the molecular director in chiral liquid-crystal phases. The mesogenic material must contain a suitable atom, that is, one with an accessible resonance energy. This condition was achieved in recent resonant diffraction studies of the different smectic mesophases by choosing sulfur-containing mesogens [7]. Our experiments established that a modulation of the orientational order takes place along the layer normal direction. The data were fully consistent with the presence of a helical symmetry axis of short pitch. This pitch was close to two-layer thicknesses in the lowest-temperature smectic C^* variant, which has antiferroelectric properties and is denoted SmC_A^*. The corresponding helical axis is 2_1. At higher temperature, there were two subphases with ferrielectric properties (SmC_{FI1}^* and SmC_{FI2}^*) corresponding to a three-layer and four-layer periodicity, respectively, i.e., 3_1 (or 3_2) and 4_1 (or 4_3) axes. The highest-temperature SmC^* variant, called SmC_α^*, had an incommensurate pitch varying between five and eight layer thicknesses over our temperature window of observation. Our most recent diffraction experiments [12] have both confirmed the results reported in our earlier publication and provided additional structural information. In particular, we mention the following.

(i) The polarization of the diffracted beam agreed with a theoretical model of the smectic-C^* variants that predicted a clocklike interlayer rotation of the in-plane projection, **c**, of the molecular director [13].

(ii) Results from experiments on a second sulfur-containing compound (MHDDOPTCOB) have confirmed our analyses of the first material studied (10OTBBB1M7) [14]. Specifically, we observed the same structure in both materials for the SmC_A^* phase, as well as a four-layer superlattice for the unique SmC_{FI2}^* phase.

(iii) In the (MHDDOPTCOB) compound, the helical ordering of the SmC^* phase was also observed by resonant scattering experiments: the measured pitch was 300 nm.

However, while on the one hand the helical clock model is consistent with the macroscopic properties of the SmC_A^* and the SmC_α^* phases, on the other hand the optical and the electro-optical properties of the SmC_{FI}^* phases are not consistent with a perfect helical ordering [4].

Different models were previously proposed for the chiral smectic-*C* variants which fit better with their macroscopic properties. Models based upon a double-layer unit cell can be easily ruled out [15]. However, some proposed models are based upon a superlattice of three- or four-layer periodicity [16]. These models, which will be described in the subsequent sections of this paper, are based upon an asymmetric unit of two, three, or four layers. Such structures are not confirmed by conventional x-ray-diffraction experiments (i.e., nonresonant satellites must be seen, while none have ever been experimentally detected). However, in order to rule out definitively these models, we will compare the resonant and the nonresonant components of the satellite peaks associated with these proposed structures. It is important to realize that these first successful resonant scattering experiments demonstrate a novel and unique technique for the investigation of chiral materials: phases with orientational order of very short and intermediate pitch can be studied under different conditions, including the effect of external strains.

In light of the need to determine the most successful model for the chiral smectic-*C* variant structures, a comparison between the structure factors of various periodic, orientational-order superlattices is needed. As a matter of fact, the structure factors of the forbidden reflections had already been estimated by Dimitrienko [17] for the case of the crystallographic nonsymmorphic symmetry elements (glide plane, 2_1, 3_n, 4_n, and 6_n axes). However, we will extend Dimitrienko's formulas to others structures by using a formalism which was previously applied to the case of visible light scattering by blue phases [18]. Therefore, we will be able to compare different helical structures with one another. We will also analyze the consequences of introducing distortion into the helical arrays. Finally, we will refer specifically to the previously proposed models for the smectic-*C* variants.

A brief overview of our subsequent presentation is as follows. In the first part, we consider the structure factor of a single smectic-*C* layer and discuss the influence of the symmetry properties of this layer upon the traceless part of the structure factor. Then we develop the general helical model. In the next section, we compare different models which are all based upon a four-layer unit cell. Finally, we discuss the influence of thermal fluctuations and compare the Debye-Waller factors of the different reflections.

II. TENSORIAL STRUCTURE FACTOR OF A SINGLE SMECTIC-*C* LAYER

The atomic scattering factor which links the scattered electric field to the incident one is analogous to the dielectric tensor [11,17]. Therefore the structure factor is a symmetrical tensor of rank 2 with nine components. Each term F_{ij} gives the amplitude of scattered *j*-polarized radiation for incident *i*-polarized radiation. Moreover, the molecular structure factor is a sum of the usual scalar structure factor *F*, which takes into account the structure of the whole molecule and of a traceless tensor f_{ij}, which depends only on the resonant atom and on the orientation of its valence orbitals within the molecule. The two terms vary in different ways close to an absorption edge. While $|F|$ decreases in the vicinity of the absorption edge, the f_{ij} tensor elements become

nonzero only within a narrow energy band around the resonant energy. The intensity of the reflections which obey the extinction rules due to the nonsymmorphic symmetry elements is proportional to $|F|^2$, whereas the intensity of the forbidden reflections (forbidden in nonresonant conditions) depends on the individual f_{ij} values. In the following, we will consider in more detail the traceless tensorial component of the structure factor.

A smectic-*C* layer of nonchiral molecules has two kinds of symmetry elements (Fig. 1): twofold rotation axes lying in the median plane of the layer, perpendicular to the director **n** and to the layer normal; and mirror planes perpendicular to the twofold axes. If the smectic layer contains chiral molecules, the mirror planes are suppressed. Let us define a set of rectangular axes. The *xy* plane is parallel to the layer plane and *y* is parallel to the twofold axis. A rotation of π around *y* transforms f_{xy} into $-f_{xy}$ and f_{yz} into $-f_{yz}$, whereas the other f_{ij} remain the same. Therefore, for a smectic-*C* phase, the resonant component of the structure factor has only three independent terms:

$$\bar{\bar{f}}=\begin{pmatrix} f_{xx} & 0 & f_{xz} \\ 0 & f_{yy} & 0 \\ f_{xz} & 0 & -(f_{xx}+f_{yy}) \end{pmatrix}. \tag{1}$$

As this tensor is unchanged under the mirror symmetry operation, the structure factors of the two enantiomers are identical.

The *xyz* coordinate system linked to the layer is convenient for looking at the modification induced by operations, such as a rotation, that act directly on the layer. However, in order to compare different phases, coordinates linked to the symmetry axes of the molecule are better. In the smectic-*C* phase, the molecule has an orthorhombic symmetry, and the tensor in this molecular frame has no off-diagonal terms and no trace. It reads

$$\bar{\bar{f}}_m=\begin{pmatrix} -f/3-\Delta & 0 & 0 \\ 0 & -f/3+\Delta & 0 \\ 0 & 0 & 2f/3 \end{pmatrix}. \tag{2}$$

$2f/3$ is the component along the director **n** and Δ measures the anisotropy in the plane perpendicular to **n**. At the Sm*C*-Sm*A* transition $\Delta\to 0$. In order to return to the reference coordinates (*xyz*) attached to the layer, we have to apply a rotation around the *y* axis of angle $-\beta$ (β is the tilt angle and goes to 0 in the Sm*A* phase). Then

$$\bar{\bar{f}}=\begin{pmatrix} (2f/3)-(f+\Delta)\cos^2\beta & 0 & \frac{1}{2}(f+\Delta)\sin 2\beta \\ 0 & -f/3+\Delta & 0 \\ \frac{1}{2}(f+\Delta)\sin 2\beta & 0 & (2f/3)-(f+\Delta)\sin^2\beta \end{pmatrix}. \tag{3}$$

In order to compare the structure factor of a sequence of smectic-*C* layers related to each other by a rotation around *z*, it is convenient to use a basis of five tensors:

$$\eta_0=\begin{pmatrix} -1 & 0 & 0 \\ 0 & -1 & 0 \\ 0 & 0 & 2 \end{pmatrix}, \quad \eta_1=\begin{pmatrix} 0 & 0 & 1 \\ 0 & 0 & i \\ 1 & i & 0 \end{pmatrix},$$

$$\eta_2=\begin{pmatrix} 1 & i & 0 \\ i & -1 & 0 \\ 0 & 0 & 0 \end{pmatrix}, \quad \eta_{-1}=\eta_1^*, \quad \eta_{-2}=\eta_2^*. \tag{4a}$$

A rotation of ψ around *z* results in a simple multiplication of these basis tensors by a complex number:

$$\eta_s\to e^{is\psi}\eta_s. \tag{4b}$$

Furthermore, in terms of these basis tensors, the structure factor of the smectic-*C* layer becomes

$$\bar{\bar{f}}=\sum_{s=-2}^{s=2} a_s\eta_s$$

with

$$\begin{aligned} a_0&=-1/2(f_{xx}+f_{yy})=f/3-1/2(f+\Delta)\sin^2\beta, \\ a_1&=a_{-1}=f_{xz}/2=1/4(f+\Delta)\sin 2\beta, \\ a_2&=a_{-2}=1/4(f_{xx}-f_{yy})=1/4\{(f+\Delta)\sin^2\beta-2\Delta\}. \end{aligned} \tag{5}$$

It is clear that the structure factors of smectic layers differing only by the direction of the projection of **n** onto the layer plane (**c**) are easy to estimate using the properties of the basis tensors (4a).

Finally, we have to define the polarization of the diffracted beam. The amplitude of a scattered wave with a unit polarization vector $\vec{e}_d$, produced by an incident beam with a unit vector of polarization $\vec{e}_i$, is $A_0\vec{e}_d\cdot\bar{\bar{f}}\vec{e}_i$, where A_0 is a constant factor which depends on the sample volume and on the amplitude of the incident beam. As we are only interested in relative amplitudes, we will ignore the term A_0 in the following discussion. In a scattering experiment, one defines the polarization by means of the unit vectors $\vec{\sigma}$ and $\vec{\pi}$, which

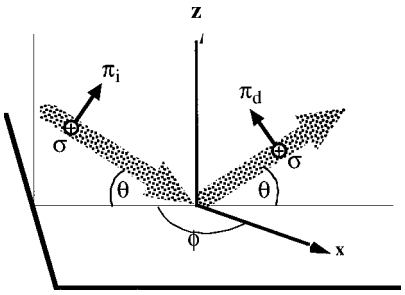

FIG. 3. Schematic representation of a diffraction experiment. The incident and scattered beams (dotted thick arrows) are in the plane of the figure; ϕ defines the orientation of the diffraction plane with respect to the sample axes x and z; the scattering vector q is parallel to z; θ is the Bragg angle.

are, respectively, perpendicular and parallel to the scattering plane (the plane defined by the incident and the scattered beams). With a $\vec{\sigma}$-polarized incident beam, the two components of the diffracted beam are $A_{\sigma\sigma}=\vec{\sigma}_d\cdot\bar{\bar{f}}\vec{\sigma}_i$ and $A_{\pi\sigma}=\vec{\pi}_d\cdot\bar{\bar{f}}\vec{\sigma}_i$, whereas with a $\vec{\pi}$ polarized incident beam the two components of the diffracted beam are $A_{\pi\pi}=\vec{\pi}_d\cdot\bar{\bar{f}}\vec{\pi}_i$ and $A_{\sigma\pi}=\vec{\sigma}_d\cdot\bar{\bar{f}}\vec{\pi}_i$, where $\vec{\sigma}_i=\vec{\sigma}_d=\vec{\sigma}$, and $\vec{\pi}_i$ and $\vec{\pi}_d$ are the unit vectors of polarization for the incident and the diffracted beams. In a layered structure (Fig. 3), the scattering plane for Bragg reflections contains the layer normal (z axis). The components of the unit polarization vectors depend on the Bragg angle θ and on the angle ϕ between the scattering plane and the x direction, which is defined to be coincident with the in-plane projector of the director, **c**. Specifically,

$$\vec{\sigma}=\begin{pmatrix}\sin\phi\\ \cos\phi\\ 0\end{pmatrix},\quad \vec{\pi}_i=\begin{pmatrix}\sin\theta\cos\phi\\ -\sin\theta\sin\phi\\ \cos\theta\end{pmatrix},$$

$$\vec{\pi}_d=\begin{pmatrix}-\sin\theta\cos\phi\\ \sin\theta\sin\phi\\ \cos\theta\end{pmatrix}.$$

Introducing the decomposition of $\bar{\bar{f}}$ into five components gives

$$\vec{\sigma}\cdot\eta_0\vec{\sigma}=1,\quad \vec{\pi}_d\cdot\eta_0\vec{\pi}_i=1+\cos^2\theta,$$

$$\vec{\sigma}\cdot\eta_0\vec{\pi}_i=\vec{\pi}_d\cdot\eta_0\vec{\sigma}=0,$$

$$\vec{\sigma}\cdot\eta_{\pm1}\vec{\sigma}=\vec{\pi}_d\cdot\eta_{\pm1}\vec{\pi}_i=0,$$

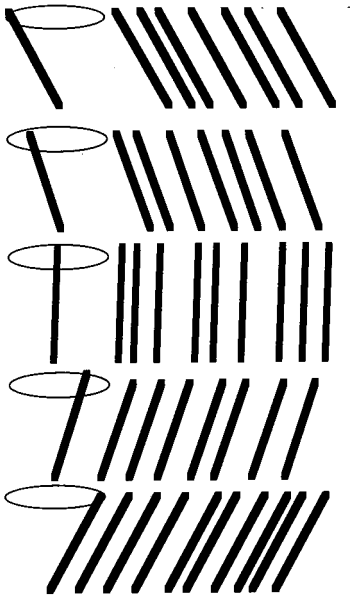

FIG. 4. Helical order in a smectic-C structure.

$$\vec{\sigma}\cdot\eta_{\pm1}\vec{\pi}_i=\vec{\pi}_d\cdot\eta_{\pm1}\vec{\sigma}=\pm i\cos\theta\exp(\mp i\phi),$$

$$\vec{\sigma}\cdot\eta_{\pm2}\vec{\sigma}=-\exp(\mp 2i\phi),\tag{6}$$

$$\vec{\pi}_d\cdot\eta_{\pm2}\vec{\pi}_i=-\sin^2\theta\exp(\mp 2i\phi),$$

$$\vec{\sigma}\cdot\eta_{\pm2}\vec{\pi}_i=-\vec{\pi}_d\cdot\eta_{\pm2}\vec{\sigma}=\pm i\sin\theta\exp(\mp 2i\phi).$$

III. RESONANT STRUCTURE FACTOR OF HELICAL STRUCTURES

A. Stacks of smectic-C layers

A helical structure is defined (Fig. 4) by the angle of rotation between two successive layers $2\pi/\nu$, where ν is the ratio between the pitch P and the layer thickness d. We consider the case of the scattering vector $\vec{Q}(h,k,l')$ parallel to z $(h=k=0)$. Introducing $l+(m/\nu)=l'$, and dropping h and k in a simplified notation, the modulus $Q(l,m)$ of the scattering vector reads $Q(l,m)=2\pi/d[l+(m/\nu)]$, where $2\pi/d$ is the unit reciprocal length parallel to z. The diffracted amplitude for a sample of N layers is

$$NF_{\rm hel}(l,m)=\sum_j e^{2\pi ij[l+(m/\nu)]}[a_0\eta_0+a_1(\eta_1e^{2\pi ij/\nu}+\eta_{-1}e^{-2\pi ij/\nu})+a_2(\eta_2e^{4\pi ij/\nu}+\bar{\bar{\eta}}_{-2}e^{-4\pi ij/\nu})]$$

$$=a_0\eta_0\sum_j e^{2\pi ij[l+(m/\nu)]}+a_1\eta_1\sum_j e^{2\pi ij[l+(m+1/\nu)]}+a_1\eta_{-1}\sum_j e^{2\pi ij[l+(m-1/\nu)]}$$

$$+a_2\eta_2\sum_j e^{2\pi ij[l+(m+2/\nu)]}+a_2\eta_{-2}\sum_j e^{2\pi ij[l+(m-2/\nu)]},$$

where j is the index of a specific layer. For large values of N the different sums are equal to zero except if the phase difference between the different terms of the sum is a multiple of 2π. For a noninteger value of ν ($\nu>1$), this condition is fulfilled only if l and m are integers with $m\leqslant 2$; $m=0$ corresponds to fundamental reflections. Consequently only four satellites are seen, two on each side of a fundamental peak. Moreover, each peak depends on only one component η_i. The amplitude of the first-order satellites, $m=1$ and -1, is described by the η_{-1} and the η_1 components, respectively; the amplitude of the second-order satellites, $m=2$ and -2, is described by the η_{-2} and the η_2 components, respectively,

$$\begin{aligned} &\text{fundamental reflections:} \quad F_{\text{hel}}(l,0)=a_0\eta_0, \\ &\text{first-order satellites:} \quad F_{\text{hel}}(l,\pm 1)=a_1\eta_{\mp 1}, \\ &\text{second-order satellites:} \quad F_{\text{hel}}(l,\pm 2)=a_2\eta_{\mp 2}. \end{aligned} \tag{7}$$

A synchrotron radiation source, such as the one used for our experiments, produces x rays linearly polarized in the electron orbit plane (which is horizontal). We also note that the layer thickness of a SmC phase is of the order of 3–4 nm, and even at low x-ray energy the Bragg angle θ is low ($\theta \leqslant 10°$). Altogether the best geometry is to have a vertical scattering plane, meaning in this case an incident $\vec{\sigma}$-polarized beam. Taking this into account, we have derived the polarization of the different resonant satellites as well as their relative intensity. The first-order satellites are $\vec{\pi}$ polarized; the diffracted beam for case $m=\pm 2$ has an elliptical polarization, but the ratio of the $\vec{\pi}$ amplitude to the $\vec{\sigma}$ amplitude is $\sin\theta$, which means that for small θ the beam is close to being $\vec{\sigma}$-polarized. The traceless part of the structure factor contributes to the fundamental reflections but does not change the polarization of the reflected beam. In fact, the scalar component of the structure factor F also depends on the energy of the incident beam when this energy approaches an absorption edge. Therefore, the intensity of the fundamental reflections has a complex dependence on the energy, which we will not consider in the following discussion.

The intensities of the satellites do not depend on the pitch value except for $\nu=2$, 3, or 4, when the amplitudes at a given resonant peak actually result from a combination of different m value reflections. Moreover, changing the handedness of the helix modifies the phases without changing the intensity of the different satellites. Taking into account Eqs. (5)–(7), the relation between the satellite intensities (assuming a $\vec{\sigma}$-polarized incident beam) and the molecular parameters f, Δ, and β is as follows.

(a) *General case* ($\nu\neq 2$, 3, *or* 4). The amplitudes are independent of ϕ, the angle between the scattering plane and the in-plane projection of the molecular director,

$$\begin{aligned} I_{l,\pm 1}&=\tfrac{1}{16}(f+\Delta)^2\sin^2 2\beta\cos^2\theta, \\ I_{l,\pm 2}&=\tfrac{1}{16}[(f-\Delta)-(f+\Delta)\cos^2\beta]^2(1+\sin^2\theta). \end{aligned} \tag{8}$$

(b) 2_1 *helical axis* ($\nu=2$). The $m=\pm 1$ reflections occur at the same wave vectors so their two amplitudes are combined and the sum depends on the angle ϕ. Assuming a random distribution of ϕ, which is defined modulo π, through the irradiated sample volume, one obtains

$$\begin{aligned} I_{l,1}&=\tfrac{1}{4}(f+\Delta)^2\sin^2 2\beta\cos^2\theta\langle\sin^2\phi\rangle \\ &=\tfrac{1}{8}(f+\Delta)^2\sin^2 2\beta\cos^2\theta. \end{aligned}$$

Notice that the $m=\pm 2$ terms give a $\vec{\pi}$ component at the fundamental reflection position. However, this component is very weak compared to the component, which results from the superposition of the dominant $m=0$ ($\vec{\sigma}$-polarized) scalar and the $m=\pm 2$ $\vec{\sigma}$-polarized resonant components.

(c) 3_1 *helical axis* ($\nu=3$). The reflections for $m=+1$ and -2, or $m=-1$ and $+2$, occur at the same wave vector and are added. The reflected beam has two components $\vec{\sigma}$ and $\vec{\pi}$. For $m=+1$,

$$F_{\sigma\sigma}=\tfrac{1}{4}[(f-\Delta)-(f+\Delta)e^{\pm 2i\phi}]$$

and

$$F_{\sigma\pi}=\frac{-i}{4}[(f-\Delta)-(f+\Delta)\cos^2\beta]\sin\theta e^{\pm 2i\phi}+\frac{i}{4}(f+\Delta)\sin 2\beta\cos\theta e^{\mp i\phi},$$

$$\begin{aligned} I_{l,\pm 1}=\tfrac{1}{16}\{&[(f-\Delta)-(f+\Delta)\cos^2\beta]^2(1+\sin^2\theta)+(f+\Delta)^2\sin^2 2\beta\cos^2\theta\} \\ &+\tfrac{1}{32}\sin 2\theta\begin{Bmatrix}\langle\cos 3\phi\rangle\sin 2\beta\,\mathrm{Re}[(f-\Delta)-(f+\Delta)\cos^2\beta](f+\Delta)^* \\ \pm\langle\sin 3\phi\rangle\sin 2\beta\,\mathrm{Im}[(f-\Delta)-(f+\Delta)\cos^2\beta](f+\Delta)^*\end{Bmatrix}. \end{aligned}$$

With the assumption of a random distribution of ϕ between 0 and $2\pi/3$,

$$\begin{aligned} I_{l,\pm 1}=\tfrac{1}{16}\{&[(f-\Delta)-1(f+\Delta)\cos^2\beta]^2(1+\sin^2\theta) \\ &+(f+\Delta)^2\sin^2 2\beta\cos^2\theta\}. \end{aligned}$$

(d) 4_1 *helical axis* ($\nu=4$). The general formula applied to the $m=\pm 1$ satellites yields

$$I_{l,\pm 1}=\tfrac{1}{16}(f+\Delta)^2\sin^2 2\beta\cos^2\theta.$$

The components $m=+2$ and -2 both contribute to the second-order satellite:

$$\begin{aligned} I_{l,\pm 2}=\tfrac{1}{4}[(f-\Delta)-(f+\Delta)\cos^2\beta]^2(&\langle\cos^2 2\phi\rangle \\ &+\langle\sin^2 2\phi\rangle\sin^2\theta). \end{aligned}$$

TABLE I. Comparison of the satellite intensities for different helical structures, assuming a collection of domains giving a random distribution of azimuthal angles. $I_{l,1}$ and $I_{l,2}$ are given by Eqs. (8).

$\|m\|$	2_1	3_1 or 3_2	4_1 or 4_3	general
1	$2I_{l,1}$	$I_{l,1}+I_{l,2}$	$I_{l,1}$	$I_{l,1}$
2[a]		$I_{l,1}+I_{l,2}$	$2I_{l,2}$	$I_{l,2}$

[a]For 3_1 and 3_2 helical axes $m=2$ is equivalent to $m=-1$.

And if ϕ is distributed at random ($0 \leqslant \phi < \pi/2$),

$$I_{l,\pm 2} = \tfrac{1}{8}[(f-\Delta)-(f+\Delta)\cos^2\beta]^2(1+\sin^2\theta).$$

In any helical structure, the intensities of the satellites, as summarized in Table I and in Fig. 5, can be compared to the satellite intensities observable from an incommensurate helical array, these intensities (general case) being labeled here as $I_{l,1}$ and $I_{l,2}$.

If the different SmC variants correspond to different helical superlattices, the intensities of the satellites remain the same, provided that the molecular conformation (and orientation of the resonant atom within the molecule) is the same in the different variants.

B. Other examples of helical mesophases

The expression of the structure factor for a helical array can be extended to the case of other helical structures, such as the cholesteric and the TGBA mesophases.

In the TGBA phase, there is up to now no clear evidence of any density modulation in a direction parallel to the helical axis [19]. However, there are periodic discontinuities of the orientation of the molecules at each grain boundary. The overall structure of the TGBA phase is that of a smectic-C phase where the grain boundaries are the layers and the director, which is the vector normal to the local slab of smectic-A layers, is parallel to the grain boundaries ($\beta = \pi/2$). In the smectic-A phase, the molecule has a uniaxial symmetry, which is reflected in the molecular structure factor ($\Delta = 0$). Therefore, if we express the structure factor of a TGBA grain in the η_s basis $\bar{\bar{f}} = \Sigma_{s=-2}^{s=2} a_s \eta_s$, then

$$a_0 = \frac{f}{3} - \tfrac{1}{2}(f+\Delta)\sin^2\beta = \frac{f}{6}, \quad a_1 = a_{-1} = \tfrac{1}{4}(f+\Delta)\sin 2\beta = 0,$$

$$a_2 = a_{-2} = \tfrac{1}{4}(f+\Delta)\sin^2\beta = \frac{f}{4}.$$

It follows from Eq. (7) that in principle there are two kinds of resonant reflections.

(i) For $Q = 2\pi/L$, where L is the distance between two grain boundaries, the structure factor of fundamental reflections is $\bar{\bar{F}}_l = \eta_0 \int_0^L dz\, e^{iQz} \rho_r(z)$, where the helical TGBA axis is coincident with the z axis and $\rho_r(z)$ is the density of resonant atoms through a TGBA grain. *For a constant density of resonant atoms the intensity of the fundamental reflections is zero.*

(ii) On each side of a fundamental reflection there is one satellite for $Q = 2\pi(l/L \pm 2/P)$ (here P is the pitch of the helical array). The structure factor of the satellites $\overline{\overline{F_{l,\pm 2}}} = \eta_{\mp 2} \int_0^L dz\, e^{i[Qz + 2\psi(z)]} \rho_r(z)$ depends on the profile $\psi(z)$ of the director orientations along the pitch direction [Fig. 6(a)]. It is interesting to discuss the limiting case where $\psi(z)$ is constant throughout the total length L of the grain, corresponding thus to abrupt grain boundaries. This case is equivalent to that of the smectic-C variants discussed in Sec. II A. However, instead of being located in narrow subsections like smectic layers, the resonant atoms are homogeneously distributed through the grain [$\rho_r(z)$ is constant]. The structure factor of the satellite is then (neglecting a phase factor) $\overline{\overline{F_{l,\pm 2}}} = \eta_{\mp 2}[2\sin(QL/2)/QL]$. The structure factor cancels for $Q = 2\pi/L$ and for $L/P \ll 1$; the satellites' intensity is weak.

(iii) The other limiting case corresponds to $\psi(z) = 2\pi z/P$, that is, to the cholesteric phase. The grain boundaries disappear with the smectic layering, and one observes

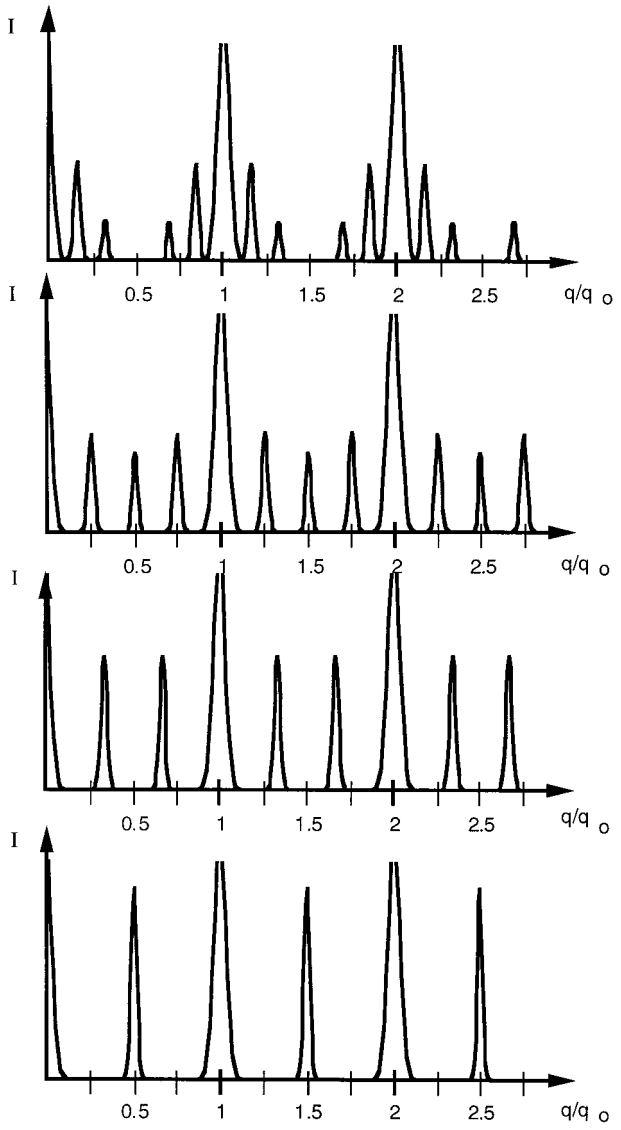

FIG. 5. Position and intensities of satellites for helical smectic phases with different pitches. From top to bottom, incommensurate pitch, four-, three-, and two-layer pitches; $q_0 = 2\pi/d$, where d is the layer thickness.

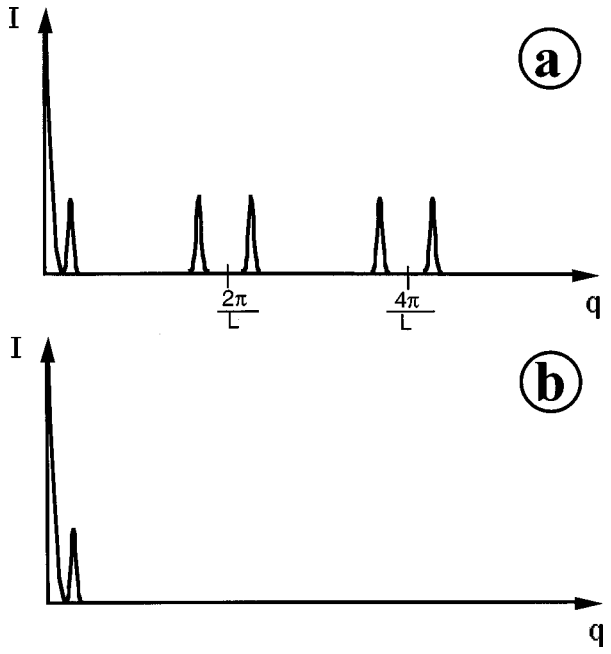

FIG. 6. Schematic representation of the satellites in the TGBA (a) and cholesteric phases (b); L is the intergrain boundaries distance; the satellites positions are $q=2\pi(l/L\pm 2/P)$, where P is the pitch of the helix.

only two peaks for $Q=\pm 4\pi/P$; their intensity is $I_s = f^2/16(1+\sin^2\theta)|\tilde{\rho}|$ [Fig. 6(b)].

IV. STRUCTURE FACTOR OF DIFFERENT MODELS BASED ON A FOUR-LAYER REPEAT UNIT

A. Description of the different models

It is clear that the clock model is consistent with the experiments performed on the smectic-*C* variants of the two studied sulfur-containing compounds. However, we must also discuss how selective the experiments are in terms of differentiating between the various proposed structures.

The basic unit of all the models is the Sm*C* layer. The repeating units are stacks of Sm*C* layers, all having, in the first approximation, the same molecular tilt angle with respect to the layer normal. The different layers within the common repeat unit differ only by the orientation of the **c** director. It is obvious that the number of possible stacking sequences increases rapidly with size of the repeat unit.

We can note at this point in the discussion that the clock model is confirmed by optical observations in the two cases when the pitch is either close to twice the layer periodicity or larger than four layers. That is, respectively, (i) for the antiferroelectric phase both in chiral and racemic mixtures [20], (ii) for the SmC^*_α phase, where the pitch derived from optical observations made on the same compound (10OTBBB1M7) is consistent with the *x*-ray data [21].

On the other hand, in the ferriphases, the presence of a 3_1 or 4_1 helical axis gives uniaxial optical properties to the basic repeat unit, and consequently the rotary power must be very low, which is not consistent with the experimental data.

In the following comparison section, we will consider only models based upon a four-layer repeat unit. In fact, the diffraction experiments made to date have revealed the existence of defects in the three-layer ferrielectric phase (SmC^*_{FI1}), since the resonant satellite peaks show a complex structure with several side bands. Moreover, the three-layer structure appears only in the 10OTBBB1M7 compound, whereas the four-layer ferrielectric phase is present in both of the compounds studied (i.e., in MHDDOPTCOB as well). In the four-layer ferrielectric phase the satellite peaks are sharp and without side bands except close to the transition to the next lower temperature mesophase range. Lastly, it is also easier to discriminate between the different models on the basis of the polarization selection rules for a four-layer structure than for a three-layer one.

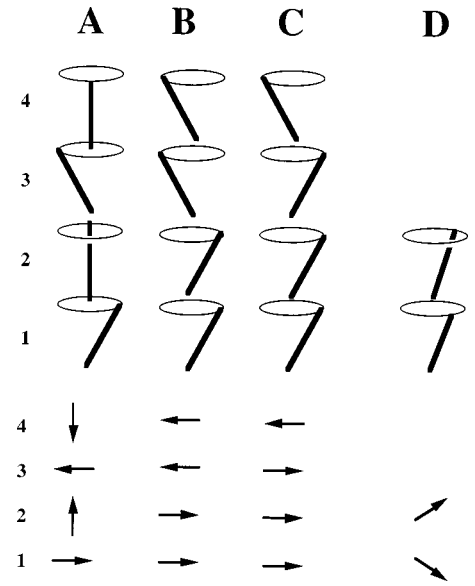

FIG. 7. Different models of two- and four-layer structures. The direction of **n** (top) and **c** (bottom) are represented in four successive layers for the clock model (*A*) [13], the *T* Ising model (*B*), and the *E* Ising model (*C*) [16], or in two layers for the distorted two-layer clock model [15].

The models described in the literature are of two classes. In the first class, the electric response of each phase is accounted for by an array of parallel or antiparallel layer dipoles (Ising models) [16]. These Ising-like models are described by a sequence of azimuthal angles ψ_i having the two values 0 and π. There are two different possible four-layer sequences $(0,0,\pi,\pi)$ and $(0,0,0,\pi)$. These two structures can be found using Landau equations for the energy in the frame of the axial next-nearest neighbor Ising (ANNI) [16] model. Each of them belongs to a different sequence of Ising-like structures depending on the external parameter which generates the sequence. For the first sequence, this is the temperature, and for the second it is an applied electric field. In the following discussion we will designate these two models as ''*T* Ising'' for the first described thermal phase sequence and ''*E* Ising'' for the second field-induced sequence (Fig. 7).

The second class of models corresponds to distorted clock models. With an even number of layers ($\nu=2n$) one can propose a symmetric sequence of angles: $2\pi j/\nu - \delta/2(-1)^j\delta/2$, with $0\leqslant j\leqslant 2n-1$. For $\nu=2$, the total dipole per unit cell is nonzero and depends on the angle δ. In fact, a two-layer distorted clock model was proposed for the ferrielectric phase [15]. However, the two layers correspond to each other by a glide mirror so that the symmetry is not

consistent with the obvious chiral properties of the ferrielectric phases. For $\nu=4$, among the different models discussed by Lorman [13b], one of them corresponds to a distorted clock model (constant tilt angle). The sequence of azimuthal angles in this distorted clock model is (Fig. 8) $(0,\pi/2-\delta,\pi,3\pi/2-\delta)$. The structure has a 2_1 symmetry, with a double-layer asymmetric unit, which corresponds, in fact, to the distorted two-layer model. Moreover, the four-layer T Ising model is a particular case of the distorted clock model with $\delta=\pi/2$. Finally, the four-layer E Ising model can be considered as a particular class of distorted clock models, where the distortion is induced by a polar stress such as that resulting from an applied dc electric field.

B. Structure factor of distorted four-layer clock models

In a four-layer superlattice there are three kinds of peaks: the fundamental peaks and the satellites of first and second order. The corresponding reciprocal vector lengths are, respectively,

$$|Q|=\frac{2\pi l}{d},\quad |Q|=\frac{2\pi}{d}(l\pm\tfrac{1}{4}),\quad |Q|=\frac{2\pi}{d}(l+\tfrac{1}{2}),$$

where d is the layer spacing and l is an integer. In this section, for convenience, we will either refer to the reflections by their (l, m) designation or by the equivalent Q/Q_0 notation $(Q_0=2\pi/d)$. In other words, the $(l, \pm1)$ reflections will also be referred to as $l\pm\frac{1}{4}$ reflections and the $(l, 2)$ reflections will also be referred to as $l+\frac{1}{2}$ reflections. We will not discuss the fundamental peaks, the intensity of which is dominated by the scalar component of the structure factor. For a sequence of azimuthal angles $(0,\psi_1,\psi_2,\psi_3)$, the first-order satellites' structure factor (per layer) is

$$\overline{\overline{F_{l,1}}}=\overline{\overline{F^*_{l,-1}}}=\frac{a_1}{4}\{\eta_1(1+ie^{i\psi_1}-e^{i\psi_2}-ie^{i\psi_3})+\eta_{-1}(1+ie^{-i\psi_1}-e^{-i\psi_2}-ie^{-i\psi_3})\}+\frac{a_2}{4}\{\eta_2(1+ie^{2i\psi_1}-e^{2i\psi_2}-ie^{2i\psi_3})+\eta_{-2}(1+ie^{-2i\psi_1}-e^{-2i\psi_2}-ie^{-2i\psi_3})\}$$

and the second-order satellites' structure factor is

$$\overline{\overline{F_{l,2}}}=\left\{\frac{a_1}{4}\eta_1(1-e^{i\psi_1}+e^{i\psi_2}-e^{i\psi_3})+\frac{a_2}{4}\eta_2(1-e^{2i\psi_1}+e^{2i\psi_2}-e^{2i\psi_3})\right\}+\{\text{c.c.}\}.$$

In the distorted helix, the 2_1 symmetry implies that $\psi_1=\pi/2-\delta$, $\psi_2=\pi$, and $\psi_3=\pi+\psi_1$. Then in $\overline{\overline{F_{l,1}}}$ the $\eta_{\pm2}$ components cancel, whereas in $\overline{\overline{F_{l,2}}}$ it is the $\eta_{\pm1}$ components which disappear. Therefore, introducing a distortion in the helical array while keeping a 2_1 symmetry does not modify the polarization state of the satellites,

$$\begin{aligned}\overline{\overline{F_{l,1}}}&=\tfrac{1}{2}a_1\{\eta_1[1-\exp(-i\delta)]+\eta_{-1}[1+\exp(+i\delta)]\},\\ \overline{\overline{F_{l,2}}}&=\tfrac{1}{2}a_2\{\eta_2[1+\exp(-2i\delta)]+\eta_{-2}[1+\exp(2i\delta)]\}.\end{aligned}\tag{9}$$

Applying the same assumption about the geometry of the diffraction experiments as in the preceding section, we can derive the satellites' intensities from Eqs. (5), (6), and (8):

$$\begin{aligned}I_{l,1}&=\langle|a_1[\cos\theta\sin\phi+i\cos\theta\cos(\phi+\delta)]|^2\rangle\\&=a_1^2\cos^2\theta\langle\sin^2\phi+\cos^2(\phi-\delta)\rangle,\\ I_{\sigma l,2}&=\langle|a_2[\cos2\phi+\cos2(\phi+\delta)]|^2\rangle\\&=4a_2^2\cos^2\delta\langle\cos^2(2\phi+\delta)\rangle,\\ I_{\pi l,2}&=4a^2\sin^2\theta\cos^2\delta\langle\sin^2(2\phi+\delta)\rangle\end{aligned}$$

assuming a random distribution of ϕ between 0 and π,

$$I_{l,1}=a_1^2\cos^2\theta=\tfrac{1}{16}(f+\Delta)^2\sin^2 2\beta\cos^2\theta,$$

$$\begin{aligned}I_{l,2}&=2a_2^2\cos^2\delta(1+\sin^2\theta)\\&=\tfrac{1}{8}\cos^2\delta(1+\sin^2\theta)[(f-\Delta)-(f+\Delta)\cos^2\beta]^2.\end{aligned}$$

From the above expressions, it is clear that the intensity of the first-order satellites is independent of the angle δ, which measures the amplitude of distortion, whereas the intensity of the second-order satellites decreases as $\cos^2\delta$. For $\delta=0$, the helical order is perfect and the structure factors are as described in Table I. For the T Ising model ($\delta=\pi/2$) *there is no resonant peak at the halfway point between two fundamental peaks*.

The introduction of some distortion in the 4_1 helical order breaks the initial symmetry. Consequently the four molecular layers which are in the same unit cell will have different electronic density profiles and the satellites will have a nonresonant component. In the model presented here, with a 2_1 symmetry axis, the nonresonant component is forbidden for odd reflections, that is, for first-order satellites. The nonresonant part of the second-order satellites will likely increase with the amplitude of the distortion. However, it is difficult to estimate the nonresonant contribution to the second-order satellite. In order to measure this contribution, it will be interesting to follow the intensity of the satellite peaks when applying a uniaxial strain compatible with the symmetry of the distortion. For example, a distortion induced by a mechanical strain or a high-frequency ac electric field, applied perpendicularly to the helical axis, would both retain the 2_1 symmetry axis.

The influence of a dc applied electric field results in a less symmetrical model (Fig. 8). Assuming that the electric field is parallel to the y axis, the sequence $(0,\pi/2,\pi,3\pi/2)$ of a perfect helical array might transform itself into the sequence $(0,\pi/2-\delta,\pi,3\pi/2+\delta)$. The E Ising model corresponds to $\delta=\pi/2$. As there is no symmetry element parallel to z, nonresonant components must be observed for $l\pm\frac{1}{4}$ and $l+\frac{1}{2}$. There are also resonant components which are

$$\begin{aligned}\overline{\overline{F_{l,1}}}&=\tfrac{1}{2}a_1\{\eta_1[1-\cos\delta]+\eta_{-1}[1+\cos\delta]\}+\tfrac{1}{2}a_2(-\eta_2+\eta_{-2})\sin2\delta,\\ \overline{\overline{F_{l,2}}}&=-\tfrac{1}{2}a_1(\eta_1+\eta_{-1})\sin\delta+\tfrac{1}{2}a_2(\eta_2+\eta_{-2})(1+\cos2\delta).\end{aligned}\tag{10}$$

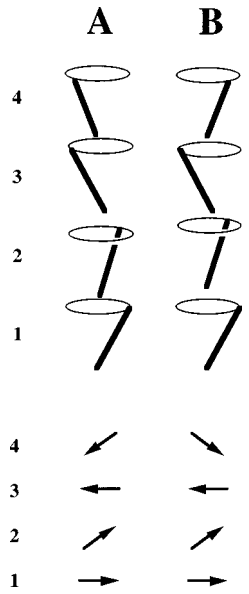

FIG. 8. Effect of a compression (*A*) or of an electric field (*B*) on the four-layer clock model (the representation conventions are the same in Figs. 7 and 8).

The two satellites have both $\vec{\sigma}$ and $\vec{\pi}$ components, except for the limit cases, i.e., for $\delta=0$ and $\delta=\pi/2$. In our experimental data, the first-order satellites are $\vec{\pi}$-polarized and the second-order satellites are $\vec{\sigma}$-polarized. In fact, it is the term in $(\eta_{+2}+\eta_{-2})$ that contributes to the $\vec{\sigma}$-polarized reflected beam. For $l\pm\frac{1}{4}$, this term cancels for $\delta=0$ and $\delta=\pi/2$; it reaches its maximum value for $\delta=\pi/4$. At the same time, for $l+\frac{1}{2}$, the $(\eta_{+2}+\eta_{-2})$ coefficient is maximum for $\delta=0$ and cancels for $\delta=\pi/2$, whereas the $(\eta_{+1}+\eta_{-1})$ term has the reverse behavior. Therefore, a measure of the polarization of the second-order satellite is a good test for the study of orientational distortions. In particular, the *E* Ising structure will give $\vec{\pi}$-polarized satellites of equal intensity for $l\pm\frac{1}{4}$ and $l+\frac{1}{2}$.

If we assume that the electric field imposes a uniform orientation of the **c** director for each layer, then the satellite intensity depends on the angle ϕ between the electric field and the normal to the scattering plane (Fig. 8). Let us give the intensity for two extreme positions of the electric field, that is, parallel or perpendicular to the scattering plane. $\phi=0$,

$$I_{\sigma\sigma}(l+\tfrac{1}{4})=0,$$

$$I_{\pi\sigma}(l+\tfrac{1}{4})=\tfrac{1}{16}\cos^2\theta(f+\Delta)^2\sin^2 2\beta\cos^2\delta,$$

$$I_{\sigma\sigma}(l+\tfrac{1}{2})=\left(\frac{f+\Delta}{2}\sin^2\beta-\Delta\right)^2\cos^4\delta,$$

$$I_{\pi\sigma}(l+\tfrac{1}{2})=0,$$

$$\phi=\pi/2,$$

$$I_{\sigma\sigma}(l+\tfrac{1}{4})=0,\quad I_{\pi\sigma}(l+\tfrac{1}{4})=\tfrac{1}{16}\cos^2\theta(f+\Delta)^2\sin^2 2\beta,$$

$$I_{\sigma\sigma}(l+\tfrac{1}{2})=\left(\frac{f+\Delta}{2}\sin^2\beta-\Delta\right)^2\cos^4\delta,\quad I_{\pi\sigma}(l+\tfrac{1}{2})=\tfrac{1}{16}\cos^2\theta(f+\Delta)^2\sin^2 2\beta\sin^2\delta.$$

It follows, then, that $\cos^2\delta$, which indicates the amplitude of the distortion, can be obtained by measuring the intensity dependence of the $I_{\pi\sigma}(l\pm\frac{1}{4})$ reflections as the direction of the scattering plane is varied with respect to the direction of the applied electric field.

Finally, it is easy to deduce the structure factor of the Lorman model from Eqs. (10) by considering the two-layer sequence $(\pi/2-\delta,3\pi/2+\delta)$ derived from the preceding four-layer structure distorted by an electric field. The first-order satellite is located at a halfway position between two fundamental peaks and, neglecting the phase factor, $\overline{\overline{F_{l,1}}}=a_1(\eta_1-\eta_{-1})\cos\delta+a_2(\eta_2-\eta_{-2})\sin 2\delta$. The structure factor cancels for $\delta=\pi/2$, that is, in the Sm*C* phase. In the antiferroelectric phase $(\delta=0)$, the reflected beam is $\vec{\pi}$-polarized. The maximum amplitude of the $\vec{\sigma}$ component is observed for $\delta=\pi/4$, that is, at the intermediate position between these two extremes.

It is clear that it is easy to discriminate between the different models by measuring the state of polarization of the different diffracted beams.

Another interesting point is the comparison of satellite intensities between phases of the same compound but with different superlattice periodicity. Such a comparison can bring to light the effects of conformational changes. It is particularly important to take into account the effect of thermal fluctuations upon the structure factor.

C. Influence of thermal fluctuations

The thermal fluctuations, specific to resonant scattering, are of two kinds.

In the first type of fluctuations, the *z* coordinate of the resonant atom deviates from its equilibrium position and the amplitude of this fluctuations increases with the temperature. The consequence is the existence of a Debye-Waller (DW) factor which multiplies the diffracted intensity otherwise obtained without fluctuations. Consequently, the intensity decreases as the reciprocal vector length increases. However, we must discriminate between the global DW factor, which takes into account fluctuations of all the atoms, and the DW factor, which is specific to the resonant atom. The first is the DW factor for the fundamental reflections, whereas the second one is appropriate for the resonant peaks.

Furthermore, the binary axis of the molecule is a consequence of an orientational disorder of the molecular director (i.e., no preferred ''up'' or ''down'' direction). If the resonant atom is far from the center of mass of the molecule, one has to consider that there are in fact two types of resonant atoms (each one contributing half of the atomic structure factor), one on each side of the median plane of the smectic layer. In such a case the satellite intensity has a sinusoidal dependence in *Q* and goes to zero for $Q=\pi/(2z_0)$, where z_0 measures the distance between the resonant atom and the center of mass of the molecule. If z_0 is large compared to the amplitude of fluctuations, the intensity of satellites with the

same m value will show a sinusoidal dependence versus the scattering vector length.

The second type of fluctuation involves changes in the **c** director. These fluctuations affect only the traceless component of the structure factor. In particular, the fluctuations of the **c** director modify the structure factor of the layers.

In order to understand this effect, consider a smectic-C layer with the **c** director parallel to x. A rotation around z of amplitude γ transforms $\bar{\bar{f}}=\Sigma_{s=-2}^{s=2}a_s\eta_s$ into $\bar{\bar{f}}_\gamma=\Sigma_{s=-2}^{s=2}e^{is\gamma}a_s\eta_s$. The mean structure factor is

$$\langle\bar{\bar{f}}\rangle=a_0\eta_0+a_1\langle\cos\gamma\rangle(\eta_1+\eta_{-1})+a_2\langle\cos 2\gamma\rangle(\eta_2+\eta_{-2}).$$

For small-amplitude fluctuations we use the approximation

$$\langle\cos\gamma\rangle\approx 1-\frac{\langle\gamma^2\rangle}{2}\approx e^{-1/2\langle\gamma^2\rangle}.$$

The orientational fluctuations of the **c** director do not change a_0. a_1 is reduced by a factor $e^{-1/2\langle\gamma^2\rangle}$ and a_2 by a factor $e^{-2\langle\gamma^2\rangle}$. This difference in the behavior of the different a_s coefficients is reflected in the temperature dependence of the ratio $I_{l,2}/I_{l,1}$ of the intensity of the second-order satellite to that of the first one. For example, in a helical array, the fluctuations of the azimuthal angle reduce the ratio by a factor $e^{-3/2\langle\gamma^2\rangle}$, whereas in the E Ising model this ratio is temperature independent.

The decay of Bragg peak intensity induced by thermal fluctuations is balanced by the diffuse scattered intensity in between these peaks. The thermal diffuse background due to orientational fluctuations of the **c** director has a peculiar dependence on both the energy of the radiation and on the magnitude of the scattering vector Q. Specifically, the intensity of the resonant scattering background vanishes outside of a narrow band of energy surrounding the absorption threshold. Moreover, the scattering factor depends on the orientation and therefore orientational fluctuations are similar to fluctuations of chemical composition. The intensity is, in the first approximation, independent of Q, whereas the usual thermal scattering intensity is proportional to Q^2.

V. CONCLUSIONS

In liquid crystals, a periodic modulation of orientational order is not necessarily coupled to a density modulation. Among chiral smectic-C variants, differences in their observed electro-optical behavior originate in differences in the structure of modulations of the c director in a direction normal to the smectic planes. Resonant x-ray-scattering experiments are able to reveal these orientational modulations. Each structure is characterized by the positions, the intensities, and the polarizations of the resonant diffraction peaks. These characteristics depend on the molecular tensorial structure factor. In order to discriminate between different models, we have extended the theory of resonant scattering developed for crystals [17]. When the traceless part of the structure factor is decomposed in a basis of five tensors which transform simply by a rotation around the layer normal, then it is straightforward to predict the structure factor for any of the SmC^* variant models proposed to date.

The simplest model of orientational modulation is the clock model [13] in which $\Delta\psi$, the angle between the **c** director of two adjacent smectic layers, is constant. In this model there is no restriction upon the period of the orientational order, which could be commensurate or incommensurate with respect to the layer periodicity. The fundamental $(l,m=0)$ reflections (coming from the layer periodicity) are surrounded on each side by two satellites with indices $m=\pm 1$ and ± 2. The intensity is independent of the period of the clock model and the $m=\pm 1$ diffracted and incident beams are cross-polarized relative to one another.

Let us compare the theoretical predictions to the experimental data [7,12]: A complete series of data, including the state of polarization of the resonant peaks, has been obtained from a chiral compound 10OTBBB1M7 [14]. Four different phases have been studied. All the observed peaks, except those corresponding to the layer structure, disappear if one moves away from the resonance energy. It is easy to compare the measured position of the observed resonant peaks with the schematic view shown in Fig. 5. The period of the helical structure is close to twice the layer periodicity in the SmC_A^* mesophase. The $m=\pm 1$ satellites are visible, but we could not see the $m=\pm 2$ satellites, which should appear as side bands around the fundamental reflections. The incident beam is $\vec{\sigma}$-polarized and polarization measurements probe the $\vec{\pi}$ state of the $m=\pm 1$ satellites. On heating the compound 10OTBBB1M7, the helical period jumps from 2 to 3 in the SmC_{FI1}^* phase and from 3 to 4 in the SmC_{FI2}^* phase. The period of the helical order appears to be commensurate (within our experimental resolution). In the SmC_{FI1}^* phase, each resonant peak is a combination of the $\eta_{\pm 1}$ and of the $\eta_{\mp 2}$ components; however, the satellites are in practice almost completely $\vec{\pi}$-polarized. In the SmC_{FI2}^* phase the $(l,2)$ and $(l+1,-2)$ components add to one another in a unique $\vec{\sigma}$-polarized peak; its intensity is about one order of magnitude lower than that of the $m=\pm 1$ peaks, which are $\vec{\pi}$-polarized. At higher temperature, we enter into the SmC_α^* phase where only one satellite is observed, which is $\vec{\pi}$-polarized. In this phase, the period of the helical array varies from 5 to 8 continuously.

All these data are consistent with a clock model. The relative intensities of the two kinds of satellites are also in keeping with the clock model: in the SmC_{FI2}^* phase, the $m=2$ satellites' intensity is weak, and they are $\vec{\sigma}$-polarized. The same $m=\pm 2$ satellites are not visible in the vicinity of the fundamental reflections in the SmC_A^* phase, because of their low intensity. In the SmC_α^* phase, the absence of $m=\pm 2$ satellites is likely a consequence of large-amplitude fluctuations of the **c** director. In the SmC_{FI1}^* phase, the $\vec{\pi}$ polarization of the satellites is also a consequence of the weak intensity of the $\vec{\sigma}$-polarized $\eta_{\mp 2}$ term.

The different phase transitions correspond to jumps of the helical periodicity (that is, the period of the clock model). The helical periodicity is incommensurate with respect to the layer thickness in the SmC_A^* and in the SmC_α^* phases. In SmC_A^*, $\Delta\psi$, the per-layer increment angle of the director **c**, is equal to $\pm\pi(1-2\varepsilon)$. The value of ε which is derived from the splitting between the (1,2) and the (2,−2) peaks is consistent with the value of the apparent optical pitch, $P_0=d/\varepsilon$ [22], where d is the layer thickness. In the SmC_α^* phase as well, the helical pitch values agree with the optical

observations [21]. In the two ferriphases there is no apparent discommensuration. Furthermore, the SmC_A phase of a racemic mixture has a helical periodicity of exactly two layers, which is consistent with the absence of chirality. Moreover, the satellites $m=\pm 1$ are $\vec{\pi}$-polarized, proving that the structure of the racemic mixture is identical to that of the enantiomer. The distorted two-layer model [15] does not apply to the racemic SmC_A phase.

The experiments performed on the compound MHDDOPTCOB [14] give similar results. The compound has SmC_A^*, SmC_{FI1}^*, and SmC^* phases. The difference in the position of the sulfur atoms in the two studied materials results in a difference in satellite intensities relative to that of the fundamental reflections. For MHDDOPTCOB in the SmC_{FI1}^* phase, the period of the helical array is close to four, but the (1,2) and the (2,−2) satellites are clearly separated, at least close to the upper and lower limits (in temperature) of the phase.

For three different smectic-C variants, SmC_A^*, SmC^*, and SmC_α^*, resonant scattering experiments confirm the helical structures (clock model), which were previously deduced from various optical observations. For the SmC_{FI}^* phases, our observations are also consistent with the clock model. It remains for us to check that this model is the only one which fits with the data. The discussion is not so obvious, at least for the SmC_{FI1}^* case: we have only one example of this phase, moreover the satellites present a substructure which is not yet understood. Furthermore, the polarization studies are not selective with respect to different proposed three-layer models.

For SmC_{FI2}^*, it is easier to discriminate between the different models based upon a four-layer superlattice. From an experimental point of view, we have two examples of this phase, one giving some evidence of a discommensurate period, even though it remains very close to 4. Furthermore, the different peaks ($m=0,1,2$) are well-separated from each other and lack detailed substructure; consequently, they are easy to characterize.

Let us first consider a period of exactly four layers. The Ising models do not fit with our observations. In the T Ising model there is no resonant peak for $m=2$ and moreover the symmetry implies a nonresonant peak at this position, which we do not see. For the E Ising model, the $m=2$ peak must be $\vec{\pi}$-polarized and a nonresonant component will be present at each position. Experimentally, the $m=2$ satellite has only a *resonant* component, which is *$\vec{\sigma}$-polarized*. The results thus contradict both Ising models.

A polar distortion of the helical array will modify the polarization state of the satellites and can therefore be easily ruled out. A nonpolar distortion applied to the four-layer clock model does not modify the polarization of the resonant peaks. However, the intensity of the $m=2$ resonant component decreases as the distortion increases and cancels for the T Ising model. For a commensurate four-layer structure, it is necessary to compare the intensity of equivalent peaks in the phases of different periods in order to detect the presence of apolar distortions; for example, one can consider that the SmC_A^* and the SmC^* phases are not distorted. However, we do not yet have sufficient information about these intensities. The maximum and the width of each peak have to be measured with more accuracy. Moreover, we must measure the influence of the partition of the resonant atoms inside a layer upon the intensities of the resonant peaks. Therefore, it is necessary to measure the intensities for different values of l, but the same m value.

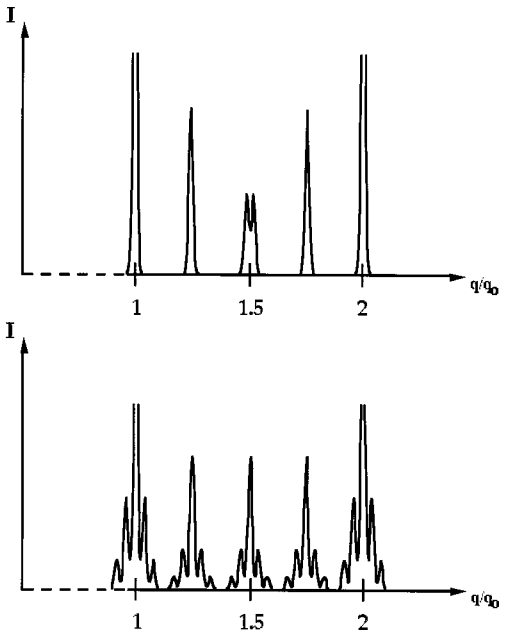

FIG. 9. Comparison of the experimental diffraction pattern of the MHDDOPTCOB in the SmC_{FI}^* phase (top) with the predicted diffraction pattern for a helical array of four-layer subunits similar to those described in Figs. 7 and 8.

Finally, it is interesting to see how the distorted models can accommodate incommensurability such as was measured in the SmC_{FI2}^* phase of MHDDOPTCOB. The distorted models are intrinsically commensurate models. It is possible to add a global chirality by keeping the original unit of a small integer number of layers (for example, four layers) and to apply chirality to the superlattice unit cell. The sequence is then $0,\pi/2-\delta,\pi,3\pi/2-\delta,\psi,\pi/2-\delta+\psi,\pi+\psi,3\pi/2-\delta+\psi,2\psi,\pi/2-\delta+2\psi,\pi+2\psi,3\pi/2-\delta+2\psi,\ldots(|\psi|\ll|\delta|)$. In this sequence a third periodicity is introduced so that two extra side peaks will be added on each side of each resonant peak (fundamental and satellites). This is not consistent with the experimental diffraction pattern of the ferri-II phase of MHDDOPTCOB (Fig. 9). In fact, the mean rotation angle between the layer j, and the layer $j+4$ is different from 2π as shown by the observed splitting of the $(l,2)$ and $(l+1,-2)$ satellites.

A slight distortion of the perfect incommensurate helical order would correspond to the following sequence: $0,\pi/2+\alpha_1\psi,\pi+\alpha_2\psi,3\pi/2+\alpha_3\psi,2\pi+\psi,\ldots$ (with $\alpha_j\neq j/4$). This is equivalent to $0,\pi/2+\delta_1,\pi+\delta_2,3\pi/2+\delta_3,2\pi+\delta_4,\ldots$, where there is no relation between δ_j and δ_{j+1} or δ_{j+2}, as is the case for a perfect incommensurate helicoidal axis or if there is a 2_1 symmetry. Therefore there does not exist a fixed angular difference $(\delta_{j+4}-\delta_j)=\psi$ between any layer j and the layer $j+4$ in the whole sample. In other words, the correlation length of a distorted incommensurate helical structure is limited by $\Delta\psi$ fluctuations.

Alternatively, the discommensuration might result from the introduction, at random, of defect layers in a commensu-

rate four-layer superlattice. This can be done in any of the four-layer models including the commensurate helicoidal structures. The sequence of azimuthal angles would then be $\psi_0, \psi_1, \psi_2, \psi_3, \ldots, (\psi_n + \delta), (\psi_{n+1} + \delta), \ldots$ with $\psi_j = \psi_{j+4}$. The mean angle of rotation per layer is $\pi/4 + \delta(N_d/N)$, where N_d/N is the proportion of defect layers. If δ is large, a small number of defect layers is enough to create a measurable incommensurability. In such a case, the presence of defects might be difficult to detect by *x*-ray diffraction.

X-ray diffraction performed in resonant conditions is a powerful method for structural determination of the structure of chiral molecules [11]. The application of this method to liquid-crystalline phases is fundamental since it is possible to reveal periodicity in the molecular orientational order. Moreover, the analysis of the polarization of the diffracted beam offers an easy way of selection between different models.

ACKNOWLEDGMENTS

We would like to acknowledge P. Barois, M. Cepic, E. Demikhov, I. Dosov, A. Fukuda, G. Joly, V. Lorman, P. Mach, S. Pikin, R. Pindak, and B. Zeks for enlightening discussions about the various structures.

[1] R. B. Meyer, L. Liébert, L. Strzelecki, and P. Keller, J. Phys. (France) Lett. **36**, 69 (1975).

[2] H. Stegemeyer, Blumel Th., K. Hiltrop, H. Onusseit, and F. Porsch, Liq. Cryst. **1**, 1 (1986).

[3] S. R. Renn and T. C. Lubensky, Phys. Rev. A **38**, 2132 (1988); Mol. Cryst. Liq. Cryst. **209**, 349 (1991); S. R. Renn, Phys. Rev. A **45**, 953 (1992); L. Navailles, R. Pindak, P. Barois, and H. T. Nguyen, Phys. Rev. Lett. **74**, 5224 (1995).

[4] (a) M. Fukui, H. Orihara, Y. Yamada, N. Yamamoto, and Y. Yshibashi, Jpn. J. Appl. Phys., Part 2 **28**, L849 (1989); (b) A. D. L. Chandani, E. Gorecka, Y. Ouchi, H. Takezoe, and A. Fukuda, *ibid.* **28**, L1265 (1989); (c) K. Hirakora, A. Taguchi, Y. Ouchi, H. Takezoe, and A. Fukuda, *ibid.* **29**, L103 (1990).

[5] A.-M. Levelut, E. Hallouin, D. Bennemann, G. Heppke, and D. Lötzsch, J. Phys. II **7**, 981 (1997).

[6] P. E. Cladis, T. Garel, and P. Pieranski, Phys. Rev. Lett. **57**, 2841 (1986); P. Pieranski and P. E. Cladis, Phys. Rev. A **35**, 355 (1987).

[7] P. Mach, R. Pindak, A.-M. Levelut, P. Barois, H. T. Nguyen, C. C. Huang, and L. Furenlid, Phys. Rev. Lett. **81**, 1015 (1998).

[8] *International Tables for Crystallography (Vol. A)*, edited by T. Hahn, D. Reidl (Dordrecht, 1983).

[9] W. Cochran, F. H. Crick, and V. Vand, Acta Crystallogr. **5**, 581 (1952).

[10] D. H. Templeton and L. K. Templeton, Acta Crystallogr., Sect. A: Found. Crystallogr. **42**, 478 (1986).

[11] D. H. Templeton and L. K. Templeton, Acta Crystallogr., Sect. A: Cryst. Phys., Diffr., Theor. Gen. Crystallogr. **36**, 237 (1980); **38**, 62 (1982); L. K. Templeton and D. H. Templeton, Acta Crystallogr., Sect. A: Found. Crystallogr. **44**, 1045 (1988).

[12] P. Mach, R. Pindak, A.-M. Levelut, P. Barois, H. T. Nguyen, H. Baltes, M. Hird, K. Toyne, A. Seed, J. W. Goodby, C. C. Huang, and L. Furenlid, preceding paper, Phys. Rev. E **60**, 6793 (1999).

[13] (a) M. Cepic and B. Zeks, Mol. Cryst. Liq. Cryst. Sci. Technol., Sect. A **263**, 61 (1995); (b) V. L. Lorman, *ibid.* **262**, 437 (1995); (c) S. A. Pikin, S. Hiller, and W. Haase, *ibid.* **262**, 425 (1995); (d) A. Roy and N. Madushudana, Europhys. Lett. **36**, 221 (1996).

[14] The chemical structures of the two compounds 100TBBB1M7 and MHDDOPTCOB are given in Ref. [12].

[15] (a) H. Orihara and Y. Ishibashi, Jpn. J. Appl. Phys., Part 2 **29**, L115 (1990); (b) B. Zeks and M. Cepic, Liq. Cryst. **14**, 445 (1993); (c) V. L. Lorman, A. A. Bulbitch, and P. Toledano, Phys. Rev. E **49**, 1367 (1994).

[16] A. Fukuda, Y. Takanashi, T. Isokasi, K. Ishikawa, and H. Takezoe, J. Mater. Chem. **4**, 997 (1994).

[17] V. E. Dimitrienko, Acta Crystallogr., Sect. A: Found. Crystallogr. **39**, 29 (1983).

[18] V. A. Beliakov and V. E. Dimitrienko, Usp. Fiz. Nauk **146**, 369 (1985) [Sov. Phys. Usp. **28**, 535 (1985)].

[19] G. Srajer, R. Pindak, M. A. Waugh, J. W. Goodby, and J. S. Patel, Phys. Rev. Lett. **64**, 13 (1990).

[20] (a) Y. Galerne and L. Liebert, Phys. Rev. Lett. **64**, 906 (1990); **66**, 289 (1991); (b) Ch. Bahr and D. Fleigner, *ibid.* **70**, 1842 (1993).

[21] L. Détré, G. Joly, N. Isaert, V. Laux, and H. T. Nguyen (unpublished).

[22] V. Laux, N. Isaert, G. Joly, and H. T. Nguyen, Liq. Cryst. **26**, 361 (1999).